Pumping efficiency in an optically pumped rubidium beam with $\sigma+\pi$ linearly polarized counterpropagating lasers

Jin Woo Jun
Department of Computational and Electronic Physics, Inje University, Kimhae 621-749, Republic of Korea

Ho Seong Lee
Division of Electromagnetic Metrology, Korea Research Institute of Standards and Science, Taejon 305-600, Republic of Korea

(Received 19 February 1998)

We investigate the population differences between ground-state hyperfine levels ($5S_{1/2}, F=2$ and $5S_{1/2}, F=1$) of an optically pumped ^{87}Rb beam in a static magnetic field, taking into account the various kinds of atomic coherence (Zeeman, hyperfine, and optical). The pumping lasers are monochromatic and in resonance with the ($5S_{1/2}, F=1 \leftrightarrow 5P_{1/2}, F'=1$) transition. By varying the polarization configuration of the pumping lasers, we find that the pumping efficiency is substantially enhanced when a σ-polarized laser and a π-polarized laser are counterpropagating. In this case, the pumping efficiency remains high even in a weak magnetic field, which explains qualitatively experimental data reported previously from a cesium beam experiment. [S1050-2947(98)07810-X]

PACS number(s): 42.50.Gy, 42.50.Hz, 42.65.An

I. INTRODUCTION

Optically pumped atomic beam frequency standards have been studied in several laboratories [1–9]. The optical method is expected to improve the stability and the accuracy of frequency standards in comparison to the conventional method using magnets. Optical pumping by lasers induces an atomic population redistribution in hyperfine levels of the ground state of alkali-metal atoms. Since the redistribution depends on characteristics of the pumping lasers, e.g., the intensity, the polarization, the linewidth, and the optical transition, etc., we must choose appropriate pumping lasers to accumulate more atoms in one hyperfine level of the ground state.

In the case of one-laser pumping, according to the report by Avila *et al.* [10], a σ-polarized laser, tuned to the ($F=4 \leftrightarrow F'=4$) transition or to the ($F=4 \leftrightarrow F'=3$) transition of the Cs-D_2 line, is the most appropriate pumping scheme to achieve the largest population difference between the two hyperfine levels $F=4$ and $F=3$ of the ground state $5S_{1/2}$. Here, a σ-polarization is a linear polarization perpendicular to the static magnetic field, while a π-polarization is a linear polarization parallel to the static magnetic field.

However, when a σ-polarized laser is used, some atoms are not pumped in the ground state when there is a low magnetic field. This phenomenon is analyzed as the nonlinear Hanle effect originating from Zeeman coherences among the ground-state Zeeman sublevels [11]. Although an increase of the magnetic field is one way to remove the population trapping, a high magnetic field affects the microwave interaction region. Therefore, in this case, magnetic shieldings should be used to separate regions [12].

Recently, Shirley and Drullinger [13] suggested a polarization switching technique using ($\sigma+\pi$) polarization for removing the population trapping in the ground state and Lee *et al.* [14] showed experimentally that the population trapping of Cs atoms could be removed by counterpropagating ($\sigma+\pi$)-polarized lasers. In this paper, we verify theoretically the above-mentioned experimental results of Lee *et al.* [14]. For simplicity, we choose the ^{87}Rb beam instead of the Cs beam.

Over the years, the optical pumping efficiency for alkali atoms has been studied under various conditions. Clerq *et al.* [15] calculated the population difference buildup for a cesium beam pumped by two lasers under a weak magnetic field. They compared results derived from a direct phenomenological approach (rate equations) to those obtained with the Bloch equation approach. For each approach, both monochromatic and broadband excitations were considered. However, it is now well established that monochromatic excitation, under which atomic coherence plays important roles, requires Liouville or Bloch equations [16] that include density matrix elements between ground states and excited states, while broadband excitation can be calculated with rate equations [17] for the ground- and excited-state populations.

Avila *et al.* [10] used the rate equation model to calculate the population difference in a cesium beam using broadband laser diode(s) under a weak magnetic field. With a rate equation model including Zeeman coherences, Theobald *et al.* [11] investigated the population trapping by a σ-polarized broadband laser diode at a low magnetic field and found a dip in the pumping efficiency curve versus the external magnetic field. Tremblay and Jacques [18] presented a new theoretical model to evaluate the pumping efficiency of two-laser pumping schemes in a weak magnetic field, taking into account optical coherence, hyperfine and Zeeman coherences of ground and excited states, neighboring transitions, and fluctuating laser fields. Recently, Jun and Lee [19] calculated the population difference between the ground-state hyperfine levels of the ^{87}Rb atom produced by a monochromatic laser in the presence of an external magnetic field with various magnitudes. The pumping laser was σ polarized, in resonance with the ($5S_{1/2}, F=2 \leftrightarrow 5P_{1/2}, F'=1$) transition. They used the Bloch equation formalism with density matrix ele-

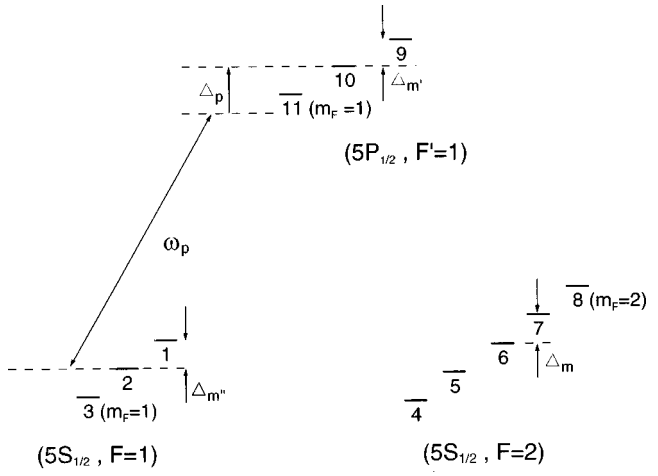

FIG. 1. Numbering convention for the D_1 line of the ^{87}Rb atom. Zeeman splittings of hyperfine levels 1, 2, and 3 are $\Delta_{m''}$, Δ_m, and $\Delta_{m'}$, respectively. Definitions of the pumping laser frequency ω_p and the pump detuning Δ_p.

ments between all the Zeeman sublevels of ground and excited hyperfine states, and consequently took into account the various kinds of atomic coherences (Zeeman coherence, hyperfine coherence, and optical coherence).

In this paper, we apply the calculation tool developed in our previous work [19] to various polarization configurations of pumping lasers that are in resonance with the $(5S_{1/2},F=1\leftrightarrow 5P_{1/2},F'=1)$ transition. However, in this work we take into account all the Bloch equations of motion between elements of the entire density matrix in contrast to our previous work, which ignored equations of motion between coherence density matrix elements.

In Sec. II, we illustrate our notations and derive equations of motion for the relevant Λ system (Fig. 1) of ^{87}Rb atoms in a static magnetic field. In Sec. III, we numerically calculate the magnetic-field dependence of the population difference under various polarization configurations and the laser intensity dependence. We also calculate the time dependence of the population difference for the counterpropagating $(\sigma+\pi)$-polarization configuration under various external magnetic fields. Discussion of the results is included in Sec. III and the conclusion follows in Sec. IV.

II. EQUATIONS OF MOTION

The master equation is the generalized Bloch equation

$$\hbar\frac{\partial}{\partial t}\hat{\rho}(t)=-i[\hat{H}(t)\hat{\rho}(t)-\hat{\rho}(t)\hat{H}(t)]-\hbar\hat{\Gamma}\hat{\rho}(t), \quad (2.1)$$

where $\hat{\rho}(t)$ is the density operator, $\hat{H}(t)$ is the Hamiltonian operator, and $\hat{\Gamma}$ describes the effects of spontaneous emission. In this paper, we consider only a specific example of the ^{87}Rb D_1 line, in which atoms in hyperfine level 1 $(5S_{1/2},F=1)$ proceed to hyperfine level 2 $(5S_{1/2},F=2)$ through hyperfine level 3 $(5P_{1/2},F'=1)$. All of these levels have magnetic sublevels that are Zeeman split by the static magnetic field. Figure 1 shows the numbering convention of this system and the Zeeman splittings $\Delta_{m''}$, $\Delta_{m'}$, and Δ_m of

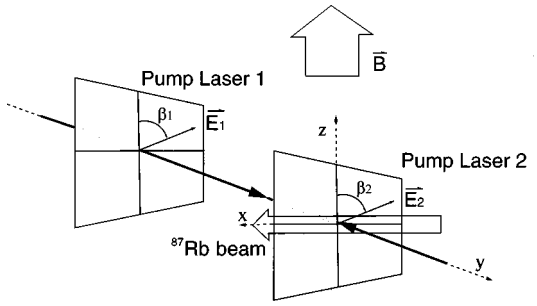

FIG. 2. Definitions of polarization angles β_1 and β_2 relative to the B field and propagation directions of laser field 1, laser field 2, and the ^{87}Rb beam.

the initial, intermediate, and final levels, respectively. The dipole moment operator of this system in the interaction picture is written as

$$\vec{\mu}=\sum_{m,n}\mu^{mn}\vec{e}_q\exp(i\omega_{mn}t)|m\rangle\langle n|, \quad (2.2)$$

where m and n denote state numbers of Fig. 1 and

$$\vec{e}_q=-\frac{i\hat{y}+q\hat{x}}{\sqrt{2}}|q|+(1-q)(1+q)\hat{z} \quad (2.3)$$

with

$$q=m_F(m)-m_F(n)=-1,\quad 0,\quad 1. \quad (2.4)$$

We set the quantization axis parallel to the z axis. The atomic transition frequency is defined such that

$$\omega_{mn}=(E_m^0-E_n^0)/\hbar, \quad (2.5)$$

where E_m^0 and E_n^0 are unperturbed energy eigenvalues of sublevels m and n. This system interacts with the pumping laser field $\vec{E}_1(\vec{r},t)$ and (or) the counterpropagating pumping laser field $\vec{E}_2(\vec{r},t)$. Figure 2 shows the situation schematically for the case where the quantization axis is parallel to the external magnetic field. In this paper, we consider only linear polarizations for both fields. In Fig. 2 we also find definitions of pump polarization angles β_1 and β_2 with respect to the B field and propagation directions of laser fields and the ^{87}Rb beam. The ^{87}Rb beam propagates in the x direction, passing through the cw pumping lasers at right angles. The total field $\vec{E}(\vec{r},t)$ is expressed as a sum of $\vec{E}_1(\vec{r},t)$ and $\vec{E}_2(\vec{r},t)$

$$\begin{aligned}\vec{E}(\vec{r},t)&=\vec{E}_1(\vec{r},t)+\vec{E}_2(\vec{r},t)\\&=\tfrac{1}{2}E_1(t)\hat{e}_1\exp(-i\omega_1t+k_1y)\\&\quad+\tfrac{1}{2}E_2(t)\hat{e}_2\exp(i\omega_2t+k_2y)+\text{H.c.}\end{aligned} \quad (2.6)$$

where $\hat{e}_1$ and $\hat{e}_2$ are polarization unit vectors, ω_1 and ω_2 are angular frequencies, and k_1 and k_2 are wave numbers of corresponding fields. In this paper, we consider the case that $\omega_1=\omega_2=\omega_p$ and consequently $k_1=k_2=k_p$. We generally start with the nonvanishing pump detuning Δ_p.

Using basis vectors $|m\rangle$, the generalized Bloch equation can be expressed as the equation for the density matrix element,

$$\frac{\partial}{\partial t}\rho_{mn}(t)=-\frac{i}{\hbar}\sum_{l=1}^{11}[H_{ml}(t)\rho_{ln}(t)-\rho_{ml}(t)H_{ln}(t)]+\left(\frac{\partial}{\partial t}\right)_{sp.}\rho_{mn}(t). \quad (2.7)$$

Now,

$$\hat{H}(t)=\hat{H}_d(t)+\hat{H}_z(t)=-\vec{\mu}\cdot\vec{E}(\vec{r},t)-\vec{\mathcal{M}}\cdot\vec{B}. \quad (2.8)$$

Matrix elements of the electric dipole interaction Hamiltonian, $H^d_{mn}(t)$, become, in the rotating-wave approximation (RWA):

$$H^d_{mn}(t)=\langle m|-\vec{\mu}\cdot\vec{E}(\vec{r},t)|n\rangle=-\mu^{mn}\exp[i\omega_{mn}(t)]^{\frac{1}{2}}\exp(i\omega_p t)\vec{e}_q\{\exp(ik_p y)\times E_2(t)\hat{e}_2+\exp(-ik_p y)E_1(t)\hat{e}_1\}. \quad (2.9)$$

Since the pumping lasers induce an optical transition between hyperfine level 1 and hyperfine level 3, the matrix elements $H^d_{mn}(t)$ $(m<n)$ are nonzero only when $1\leqslant m\leqslant 3$ and $9\leqslant n\leqslant 11$. Matrix elements $H^d_{mn}(t)$ can be expressed using polarization angles instead of polarization unit vectors like $H^d_{1,9}(t)$,

$$\frac{1}{\hbar}H^d_{1,9}(t)\exp(i\Delta_p t)=-\frac{1}{2\hbar}\mu^{1,9}\{\exp(ik_p y)E_2(t)\cos\beta_2+\exp(-ik_p y)E_1(t)\cos\beta_1\}. \quad (2.10)$$

Now, dipole components $\mu^{1,9}$ can be further expressed [15] by use of the Wigner-Eckart theorem as

$$\mu^{1,9}=\langle J_1||\mu||J_9\rangle(-1)^{1+I+J_9+F_9+F_1-m_{F9}}\times(2F_9+1)^{1/2}(2F_1+1)^{1/2}\times\begin{pmatrix}F_9 & 1 & F_1\\ -m_{F9} & q & m_{F1}\end{pmatrix}\begin{Bmatrix}F_9 & 1 & F_1\\ J_1 & I & J_9\end{Bmatrix}=\langle J_1||\mu||J_9\rangle C(1,9), \quad (2.11)$$

where $\langle J_1||\mu||J_9\rangle$ is proportional to the reduced matrix element and () and {} are, respectively, $3j$ and $6j$ symbols that can be obtained from standard tables.

Using definitions

$$-\frac{E_1(t)}{\hbar}\langle J_1||\mu||J_9\rangle=\Omega_1(t) \quad (2.12)$$

and

$$-\frac{E_2(t)}{\hbar}\langle J_1||\mu||J_9\rangle=\Omega_2(t), \quad (2.13)$$

Equation (2.10) becomes

$$\frac{1}{\hbar}H^d_{1,9}(t)\exp(i\Delta_p t)=\tfrac{1}{2}C(1,9)\{\exp(ik_p y)\Omega_2(t)\cos\beta_2+\exp(-ik_p y)\Omega_1(t)\cos\beta_1\}. \quad (2.14)$$

Similarly,

$$\frac{1}{\hbar}H^d_{1,10}(t)\exp(i\Delta_p t)=\tfrac{1}{2}C(1,10)\frac{1}{\sqrt{2}}\{-\exp(ik_p y)\Omega_2(t)\sin\beta_2-\exp(-ik_p y)\Omega_1(t)\sin\beta_1\}. \quad (2.15)$$

To simplify expressions we use definitions

$$\mathcal{C}(y,t)=\exp(ik_p y)\Omega_2(t)\cos\beta_2+\exp(-ik_p y)\Omega_1(t)\cos\beta_1 \quad (2.16)$$

and

$$\mathcal{S}(y,t)=-\exp(ik_p y)\Omega_2(t)\sin\beta_2-\exp(-ik_p y)\Omega_1(t)\sin\beta_1. \quad (2.17)$$

Here we use the written letter $\mathcal{C}$ to avoid confusion with the coefficient $C(m,n)$ of Eq. (2.11). Then,

$$\frac{1}{\hbar}H^d_{1,9}(t)\exp(i\Delta_p t)=\tfrac{1}{2}\mathcal{C}(y,t) \quad (2.18)$$

and

$$\frac{1}{\hbar}H^d_{1,10}(t)\exp(i\Delta_p t)=\frac{1}{2\sqrt{2}}\mathcal{S}(y,t). \quad (2.19)$$

The remaining nonvanishing matrix elements $H^d_{m,n}(t)$ $(m<n)$ are

$$\frac{1}{\hbar}H^d_{2,9}(t)\exp(i\Delta_p t)=\frac{1}{2\sqrt{2}}\mathcal{S}(y,t),$$
$$\frac{1}{\hbar}H^d_{2,11}(t)\exp(i\Delta_p t)=\frac{1}{2\sqrt{2}}\mathcal{S}(y,t),$$
$$\frac{1}{\hbar}H^d_{3,10}(t)\exp(i\Delta_p t)=\frac{1}{2\sqrt{2}}\mathcal{S}(y,t), \quad (2.20)$$
$$\frac{1}{\hbar}H^d_{3,11}(t)\exp(i\Delta_p t)=\tfrac{1}{2}\mathcal{C}(y,t).$$

On the other hand, matrix elements of the Zeeman interaction Hamiltonian, $H^z_{mn}(t)$, survive the RWA only if m is equal to n such that

$$\frac{1}{\hbar}H^{z}_{mn}(t)=\frac{1}{\hbar}\langle m|-\vec{\mathcal{M}}\cdot\vec{B}|n\rangle \tag{2.21}$$

$$=\begin{cases}\dfrac{-1}{2}\dfrac{\mu_B B}{\hbar}m_F(n)=-\Delta_{m''}m_F(n) & \text{when } 1\leqslant n\leqslant 3\\ \dfrac{1}{2}\dfrac{\mu_B B}{\hbar}m_F(n)=\Delta_m m_F(n) & \text{when } 4\leqslant n\leqslant 8\\ \dfrac{-1}{6}\dfrac{\mu_B B}{\hbar}m_F(n)=-\Delta_{m'}m_F(n) & \text{when } 9\leqslant n\leqslant 11.\end{cases} \tag{2.22}$$

If we define slowly varying functions $\rho'_{mn}(t)$ from the original functions $\rho_{mn}(t)$ such that

$$\rho_{mn}(t)=\begin{cases}\rho'_{mn}(t)\exp(-i\Delta_p t) & \text{when } 1\leqslant m\leqslant 3 \text{ and } 9\leqslant n\leqslant 11\\ \rho'_{mn}(t)\exp(i\Delta_p t) & \text{when } 9\leqslant m\leqslant 11 \text{ and } 1\leqslant n\leqslant 3\\ \rho'_{mn}(t) & \text{otherwise,}\end{cases} \tag{2.23}$$

and similarly for the elements of $H'_{mn}(t)$ in terms of $H_{mn}(t)$, then Bloch equations for density matrix elements $\rho'_{mn}(t)$ can be expressed in terms of $H'_{mn}(t)$ as follows:

$$\frac{\partial}{\partial t}\rho'_{mn}(t)=i\Delta_p\rho'_{mn}(t)-\frac{i}{\hbar}\sum_{l=1}^{11}[H'_{ml}(t)\rho'_{ln}(t)-\rho'_{ml}(t)H'_{ln}(t)]+\left(\frac{\partial}{\partial t}\right)_{sp.}\rho'_{mn}(t), \tag{2.24}$$

where the term $i\Delta_p\rho'_{mn}(t)$ appears only when $1\leqslant m\leqslant 3$, $9\leqslant n\leqslant 11$ or $9\leqslant m\leqslant 11$, $1\leqslant n\leqslant 3$.

Now, decay terms due to spontaneous emission can be obtained from the master equation for an atomic system of multi-Zeeman sublevels interacting with a vacuum reservoir [16]. Using the set of indices (i,α) to denote a Zeeman sublevel m, where the index i represents the hyperfine levels and the index α represents the m_F value, results are summarized in the set of equations

$$\left(\frac{d}{dt}\right)_{sp.}\rho'_{mn}(t)=\left(\frac{d}{dt}\right)_{sp.}\rho'^{\,i,j}_{\alpha,\beta}$$

$$=\begin{cases}\displaystyle\sum_{k,q}\Gamma_{k,\alpha+q;k,\beta+q\to i,\alpha;i,\beta}\rho'^{\,k,k}_{\alpha+q,\beta+q}-\sum_{k}\Gamma_{i\to k}\rho'^{\,i,i}_{\alpha,\beta} & \text{when } i=j\\ \displaystyle -0.5\left(\sum_{k}\Gamma_{i\to k}+\sum_{k}\Gamma_{j\to k}\right)\rho'^{\,i,j}_{\alpha,\beta} & \text{when } i\neq j.\end{cases} \tag{2.25}$$

Furthermore,

$$\Gamma_{i\to k}=\Gamma_{i,k}\sum_{q}C((i,\alpha),(k,\alpha+q))\times C((i,\alpha),(k,\alpha+q)) \tag{2.26}$$

and

$$\Gamma_{k,\alpha+q;k,\beta+q\to i,\alpha;i,\beta}=\Gamma_{k,i}C((k,\alpha+q),(i,\alpha))\times C((k,\beta+q),(i,\beta)), \tag{2.27}$$

where

$$\Gamma_{i,j}=\begin{cases}\dfrac{|\langle J_i||\mu||J_j\rangle|^2\omega_{ij}^3}{3\pi\varepsilon_0\hbar c^3} & \text{if } i>j\\ 0 & \text{if } i<j.\end{cases} \tag{2.28}$$

From now on, for convenience, we delete the prime from $\rho'_{mn}(t)$ and $H'_{mn}(t)$. Then, for example, the Bloch equation for $\rho_{1,1}(t)$ becomes

$$\begin{aligned}\frac{\partial\rho_{1,1}}{\partial t}=&-i\left[\Delta_{m''}\rho_{1,1}+\frac{\mathcal{C}}{2}\rho_{9,1}+\frac{\mathcal{C}}{2\sqrt{2}}\rho_{10,1}-\left(\Delta_{m''}\rho_{1,1}+\frac{\mathcal{C}^*}{2}\rho_{1,9}+\frac{\mathcal{S}^*}{2\sqrt{2}}\rho_{1,10}\right)\right]\\ &+\Gamma_{2,1}C((2,-1),(1,-1))C((2,-1),(1,-1))\rho_{5,5}\\ &+\Gamma_{2,1}C((2,0),(1,-1))C((2,0),(1,-1))\rho_{6,6}\\ &+\Gamma_{3,1}C((3,-1),(3,-1))C((3,-1),(3,-1))\rho_{9,9}\\ &+\Gamma_{3,1}C((3,0),(1,-1))C((3,0),(1,-1))\rho_{10,10}\\ =&-i\left[\frac{\mathcal{C}}{2}\rho_{9,1}+\frac{\mathcal{S}}{2\sqrt{2}}\rho_{10,1}-\frac{\mathcal{C}^*}{2}\rho_{1,9}-\frac{\mathcal{S}^*}{2\sqrt{2}}\rho_{1,10}\right]\\ &+\Gamma_{3,1}\rho_{9,9}+\Gamma_{3,1}\rho_{10,10}.\end{aligned} \tag{2.29}$$

This model has 11 atomic levels and, therefore, requires 121 density matrix elements in order to describe its dynamics fully. Since the density matrix is Hermitian, there are 66 independent matrix elements. We display the remaining 65 coupled differential equations in the APS eprint [20] for future use. Since the system is closed, the differential equations are degenerate. Therefore, we impose a constraint equation by normalizing the sum of the populations.

III. NUMERICAL SIMULATIONS AND DISCUSSION

Although we generally construct Bloch equations to treat the case $\Delta_p \neq 0$, in this paper, we consider only the $\Delta_p = 0$ situation where pumping fields are in resonance with the transition between hyperfine levels 1 and 3. To solve the coupled partial differential equations, we use the subroutine imsl_f_ode_runge_kutta in the IMSL C numerical library. Since diagonal elements of the density matrix represent populations in the corresponding Zeeman sublevel, we normalize the sum of diagonal elements at each instance. We specifically choose the initial state such that the populations are statistically distributed in the ground-state hyperfine levels:

$$\rho_{1,1}(0)=\rho_{2,2}(0)=\rho_{3,3}(0)=\frac{1}{6},$$

$$\rho_{4,4}(0)=\rho_{5,5}(0)=\rho_{6,6}(0)=\rho_{7,7}(0)=\rho_{8,8}(0)=\frac{1}{10}, \tag{3.1}$$

$$\rho_{9,9}(0)=\rho_{10,10}(0)=\rho_{11,11}(0)=0.$$

Since the lasers are monochromatic, the broadband Fourier components from sudden turn-on of the lasers are negligible. Therefore, we approximate the initial situation such that the lasers suddenly turn on, i.e., we set the initial values of all off-diagonal elements to zero. In order to obtain a meaningful value at the final time T, we should average over the space because the density matrix elements depend on the position of the ^{87}Rb beam. This procedure is especially important when the ^{87}Rb beam interacts with two counterpropagating lasers. In this case, due to wave interference, the polarization of the resultant laser field varies over the y component of the ^{87}Rb beam position [21]. In this paper, we select the inverse of the spontaneous decay rate from hyperfine level 3 to hyperfine level 1, $\tau_{3,1}=1/\Gamma_{3,1}=0.176$ μs, to be the measure of the interaction time T and the saturation intensity for $5S_{1/2}\leftrightarrow 5P_{1/2}$ transition, $I_s=1.4$ mW/cm^2, to be the measure of the laser intensity I.

Figure 3 shows the magnetic field dependence of the population difference between hyperfine level 1 and hyperfine level 2. The interaction time is 10 μs ($=56.8$ $\tau_{3,1}$) and the pumping laser intensity is 0.4 mW/cm^2 ($=0.29$ I_s). Since the value of the population difference does not vary significantly after 10 μs (Fig. 6), we neglect the effect of different transverse velocities but take a fixed interaction time, 10 μs. Although the interaction time for the Cs beam experiment was 20 μs [14], we take 10 μs as an interaction time in the numerical simulation for the ^{87}Rb beam in order to show clearly the magnetic-field dependence

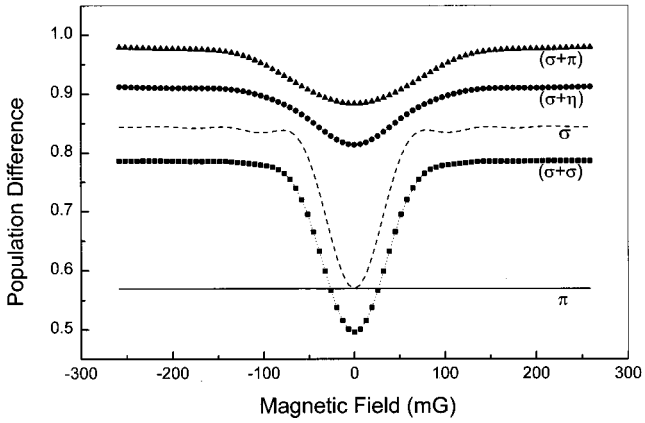

FIG. 3. Population differences between hyperfine levels 1 and 2, $P_2-P_1=(\rho_{4,4}+\rho_{5,5}+\rho_{6,6}+\rho_{7,7}+\rho_{8,8})-(\rho_{1,1}+\rho_{2,2}+\rho_{3,3})$, as a function of the magnetic field under parameters $T=10$ μs and $I=0.4$ mW/cm^2 due to a single pumping laser with $\beta_1=0$ (solid line), a single laser with $\beta_1=\pi/2$ (dashed line), two counterpropagating pumping lasers with $\beta_1=\pi/2,\beta_2=\pi/2$ (squares), $\beta_1=\pi/2,\beta_2=\pi/4$ (circles), $\beta_1=\pi/2,\beta_2=0$ (triangles).

of the pumping efficiency (Fig. 6). We calculate the population difference under five different polarization configurations of the pumping laser(s): a single laser with either π polarization ($\beta_1=0$) or σ polarization ($\beta_1=\pi/2$), and two counterpropagating lasers with either $(\sigma+\sigma)$ polarization ($\beta_1=\pi/2$, $\beta_2=\pi/2$) or $(\sigma+\eta)$ polarization ($\beta_1=\pi/2$, $\beta_2=\pi/4$) or $(\sigma+\pi)$ polarization ($\beta_1=\pi/2,\beta_2=0$), where η polarization is a linear polarization with its polarization angle $\beta=\pi/4$ relative to the static magnetic field. The curve in the case of π polarization shows no population trapping phenomenon, as expected, and the curve for the case of σ polarization shows the typical coherence dip of the Hanle effect [11,14,19]. At $B=0$ the pumping efficiency of the π-polarized laser is equal to that of the σ-polarized laser, because there is no difference between the two cases in the absence of a magnetic field.

The three new curves in the cases of $(\sigma+\sigma)$ polarization, $(\sigma+\eta)$ polarization, and $(\sigma+\pi)$ polarization all show the coherence dip of the Hanle effect. Among these three cases, the pumping efficiency of the $(\sigma+\sigma)$-polarized lasers turns out to be the lowest and is even lower than the pumping efficiency of the σ-polarized laser. The pumping efficiency of the $(\sigma+\pi)$-polarized lasers turns out to be the highest and is higher than the pumping efficiency of the σ-polarized laser. It is very noticeable that the depth of the coherence dip becomes smaller when the polarization configuration changes from $(\sigma+\sigma)$- to $(\sigma+\pi)$ polarization. Consequently, when we pump the ^{87}Rb beam with two counterpropagating $(\sigma+\pi)$-polarized lasers, we obtain the highest pumping efficiency even under a weak magnetic field.

A few years ago, this phenomenon was reported in the Cs frequency standard experiment by Lee *et al.* [14]. This is a very desirable phenomenon because we do not need to use magnetic shielding to separate the pumping region and the microwave interaction region [12].

Now, the qualitative behavior of the $(\sigma+\pi)$ curve of Fig. 3 can be compared with that of experimental data [14]. When Lee *et al.* [14] pumped a Cs beam with a $(\sigma+\pi)$-polarized laser with intensity 0.76 mW/cm^2 tuned to the $F=4\rightarrow F'$

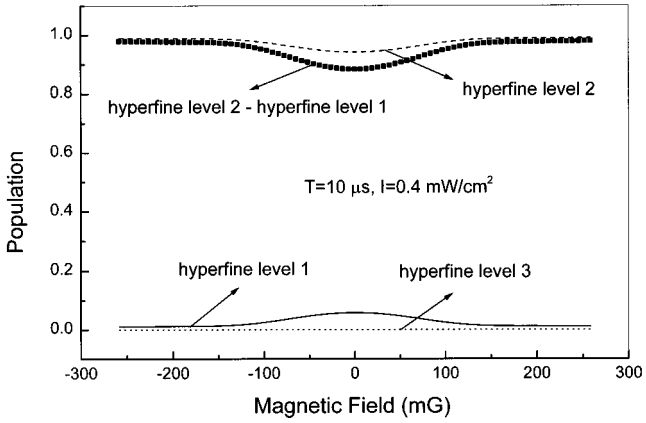

FIG. 4. Populations of hyperfine levels 1 (solid line), 2 (dashed line), and 3 (dotted line) in addition to the population difference (squares) between hyperfine levels 1 and 2, as a function of the magnetic field under parameters $T=10\ \mu$s, $I=0.4$ mW/cm^2, $\beta_1=\pi/2$, and $\beta_2=0$.

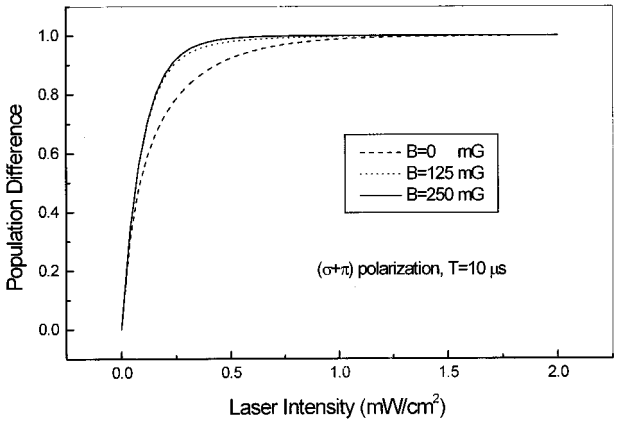

FIG. 5. Population differences between hyperfine levels 1 and 2, P_2-P_1, as a function of the intensity of $(\sigma+\pi)$ polarized lasers. $T=10\ \mu$s. The solid line, the dashed line, and the dotted line represent cases under the magnetic field $B=250$ mG, $B=125$ mG, and $B=0$ mG, respectively.

$=3$ transition, the Cs population difference was 0.98 in the presence of a strong magnetic field, ± 250 mG. In Fig. 3 the corresponding ^{87}Rb population difference also reads as 0.98 when $B=\pm 250$ mG. In the absence of the magnetic field, the Cs population difference by $(\sigma+\pi)$-polarized lasers was slightly reduced to 0.97, while the Cs population difference by the σ-polarized laser was substantially reduced to 0.70.

In the absence of a magnetic field, we can also find in Fig. 3 that the ^{87}Rb population difference for $(\sigma+\pi)$-polarized lasers is reduced to 0.88, while the ^{87}Rb population difference for the σ-polarized laser is substantially reduced to 0.57. During the experiment, the temperature of the Cs oven was set at 114 °C. The degree of vacuum inside the chamber was 5×10^{-5} Pa under the normal beam operation. The mean interaction time of Cs atoms with the laser beam was 20 μs since the mean velocity of Cs atoms is 248 m/s at 114 °C. The $(\sigma+\pi)$ polarization was made by superposing a σ-polarized laser on a π-polarized laser that was made from the incident σ-polarized laser with a quarterwave plate and a reflector placed at the site of the back window of the vacuum chamber. From now on, we restrict our attention to the $(\sigma+\pi)$-polarization configuration, as it is the most interesting one.

In Fig. 4 we show the magnetic-field dependence of the population of three relevant hyperfine levels 1, 2, and 3 in addition to the magnetic-field dependence of the population difference between hyperfine levels 1 and 2. The interaction time, 10 μs $(=56.8\ \tau_{3,1})$, and the pumping laser intensity, 0.4 mW/cm^2 $(=0.29\ I_s)$, are the same as those of Fig. 3. The population of excited hyperfine level 3 remains almost at zero as the magnetic field grows. However, the population of hyperfine level 1 (2) slowly decreases (increases) as the magnetic field grows, and consequently we observe a shallow coherence dip.

In Fig. 5, we plot the intensity dependence of the population difference between hyperfine levels 1 and 2 after 10 μs interaction time. We find that as the pumping intensity grows, the pumping efficiency grows rapidly to 1. Since the external magnetic field destroys the Zeeman coherence the pumping efficiency grows more rapidly as the external magnetic field becomes stronger.

Finally, in Fig. 6, we plot the time evolution behavior of the population difference between hyperfine levels 1 and 2 under various pumping intensities and external magnetic fields. All curves start at zero since we choose the evenly populated state as the initial state, and they grow rapidly to 1. The population difference grows more rapidly when there is a 250 mG magnetic field in comparison to the 0 mG case as in Fig. 5. However, the pumping efficiency difference between the $B=0$ mG case and the $B=250$ mG case becomes narrower as the interaction time becomes longer. This means that it is necessary to pump the ^{87}Rb beam for the longer interaction time to induce the more desirable phenomenon in the frequency standard experiment. On the other hand, the pumping efficiency difference, between the $B=0$ mG case and the $B=250$ mG case at a fixed interaction time (e.g., 10 μs), becomes narrower as the laser intensity becomes stronger. This means that it is necessary to pump the ^{87}Rb beam with a greater intensity to induce the more desirable phenomenon in the frequency standard experiment.

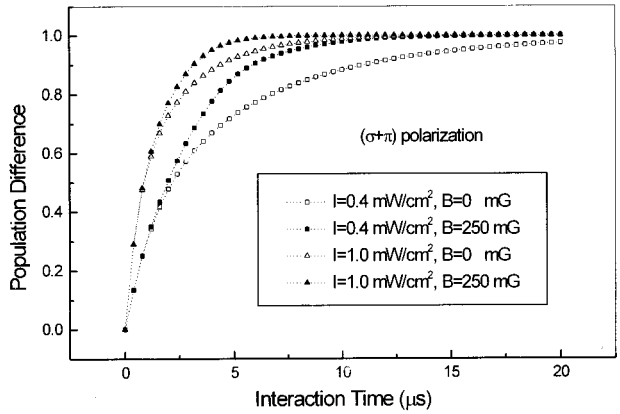

FIG. 6. Population differences between hyperfine levels 1 and 2, P_2-P_1, as a function of the interaction time of $(\sigma+\pi)$ polarized lasers. Open squares, solid squares, open triangles, and solid triangles represent cases of $(I=0.4$ mW/cm^2, $B=0$ mG), $(I=0.4$ mW/cm^2, $B=250$ mG), $(I=1.0$ mW/cm^2, $B=0$ mG), and $(I=1.0$ mW/cm^2, $B=250$ mG), respectively.

As we observed in Fig. 5, the population difference grows more rapidly when I is equal to 1.0 mW/cm^2 ($=0.71\ I_s$) in comparison to the $I=0.4$ mW/cm^2 ($=0.29\ I_s$) case.

The rate equation models treat only the populations of the sublevels, i.e., the diagonal matrix elements. Since we adopt simple initial conditions for off-diagonal elements in this Bloch equation model, the initial conditions are effectively the same as those of the rate equation models. However, since the rate equation models can only adopt the crude transit relaxation model [22], they might not explain the subtle effects discussed above.

IV. CONCLUSION

For optical pumping of a multisublevel ^{87}Rb beam in a static magnetic field by monochromatic lasers in resonance with the transition between hyperfine levels 1 and 3, we investigate numerically the population difference between ground state hyperfine levels 1 and 2 by use of the Bloch equation formalism that rigorously takes into account various atomic coherence effects. By varying the polarization configuration of the pumping lasers, we find that the pumping efficiency is substantially enhanced when we pump the ^{87}Rb beam with counterpropagating $(\sigma+\pi)$-polarized lasers. Since the coherence population trapping is removed even under a weak magnetic field, this phenomenon [14] is very desirable in the frequency standard experiment. To our knowledge, these impressive numerical findings are not predicted by any other treatment. It is also numerically confirmed that it is necessary to pump the ^{87}Rb beam by counterpropagating $(\sigma+\pi)$-polarized lasers at greater intensity for a longer interaction time in order to obtain a higher pumping efficiency with a shallower coherence dip.

Since the $(\sigma+\pi)$-polarization configuration is also used in the laser cooling method by polarization gradients [21], we plan to apply our scheme to calculate relevant physical quantities such as the radiative force, the equilibrium temperature, etc. Furthermore, it is straightforward to generalize and apply this approach to another laser cooling method by the two circular polarization configuration [21].

ACKNOWLEDGMENT

This work was supported by the Star Project (Project No. 97-NQ-05-01-A) of the Korea Ministry of Science and Technology.

[1] L. Essen, E. G. Hope, and D. Sutcliffe, Nature (London) **189**, 298 (1961).
[2] S. Pensenlin, T. Moran, V. W. Cohen, and G. Winkler, Phys. Rev. **127**, 524 (1962).
[3] M. Arditi and P. Cerez, IEEE Trans Instrum. Meas. **IM-21**, 391 (1972).
[4] E. de Clercq, G. D. Rovera, S. Bouzid, and A. Clairon, IEEE Trans Instrum. Meas. **42**, 457 (1993).
[5] N. Dimarcq, V. Giordaro, P. Cerez, and G. Theobald, IEEE Trans Instrum. Meas. **42**, 115 (1993).
[6] R. E. Drullinger, J. H. Shirley, J. P. Lowe, and D. J. Glaze, IEEE Trans Instrum. Meas. **42**, 453 (1993).
[7] S. Ohshima, Y. Nakadan, T. Ikegami, and Y. Koga, IEEE Trans Instrum. Meas. **38**, 1100 (1989).
[8] T. Maeno, H. Saito, J. Umezu, Y. Ohta, M. Kajita, R. Hayashi, and E. Morikawa, IEEE Trans Instrum. Meas. **40**, 146 (1991).
[9] D.-H. Yang and Y.-Q. Wang, Opt. Commun. **73**, 285 (1989).
[10] G. Avila, V. Giordano, V. Candelier, E. de Clercq, G. Theobald, and P. Cerez, Phys. Rev. A **36**, 3719 (1987).
[11] G. Theobald, N. Dimarcq, V. Giordano, and P. Cerez, Opt. Commun. **71**, 256 (1989).
[12] V. Giordano, A. Hamel, P. Petit, G. Theobald, N. Dimarcq, P. Cerez, and C. Audoin, IEEE Trans. Ultrason. Ferroelectr. Freq. Control **38**, 350 (1991).
[13] J. H. Shirley and R. E. Drullinger (unpublished).
[14] H. S. Lee, S. H. Yang, Y. B. Kim, J. O. Kim, and C. H. Oh, Jpn. J. Appl. Phys., Part 1 **35**, 299 (1996).
[15] E. de Clercq, M. de Labachellerie, G. Avila, P. Cerez, and M. Tetu, J. Phys. (France) **45**, 239 (1984).
[16] C. Cohen-Tannoudji, in *Frontiers in Laser Spectroscopy*, 1975 Les Houches Lectures, edited by R. Balian, S. Haroche, and S. Liberman (North-Holland, Amsterdam, 1977).
[17] M. Arditi, I. Hirano, and P. Tougne, J. Phys. D **11**, 2465 (1978).
[18] P. Tremblay and C. Jacques, Phys. Rev. A **41**, 4989 (1990).
[19] J. W. Jun and H. S. Lee, Opt. Commun. **149**, 43 (1998).
[20] J. W. Jun and H. S. Lee, http://publish.aps.org/eprint/gateway/eplist/aps1998apr17-001.
[21] J. Dalibard and C. Cohen-Tannoudji, J. Opt. Soc. Am. B **6**, 2023 (1989).
[22] J. Sagle, R. K. Namiotka, and J. Huennekens, J. Phys. B **29**, 2629 (1996).